



## Structure of $^{191}\text{Pb}$ from $\alpha$ - and $\beta$ -decay spectroscopy

T E Cocolios, a N Andreyev, S Antalic, A Barzakh, B Bastin, J Büscher, I G Darby, W Dexters, D V Fedorov, V N Fedosseev, et al.

### ► To cite this version:

T E Cocolios, a N Andreyev, S Antalic, A Barzakh, B Bastin, et al.. Structure of  $^{191}\text{Pb}$  from  $\alpha$ - and  $\beta$ -decay spectroscopy. *Journal of Physics G: Nuclear and Particle Physics*, 2010, 37 (12), pp.125103. 10.1088/0954-3899/37/12/125103 . hal-00600787

**HAL Id: hal-00600787**

**<https://hal.science/hal-00600787>**

Submitted on 16 Jun 2011

**HAL** is a multi-disciplinary open access archive for the deposit and dissemination of scientific research documents, whether they are published or not. The documents may come from teaching and research institutions in France or abroad, or from public or private research centers.

L'archive ouverte pluridisciplinaire **HAL**, est destinée au dépôt et à la diffusion de documents scientifiques de niveau recherche, publiés ou non, émanant des établissements d'enseignement et de recherche français ou étrangers, des laboratoires publics ou privés.

# Structure of $^{191}\text{Pb}$ from $\alpha$ - and $\beta$ -decay spectroscopy

T.E. Cocolios<sup>1</sup>, A.N. Andreyev<sup>1,2</sup>, S. Antalic<sup>3</sup>, A. Barzakh<sup>4</sup>,  
B. Bastin<sup>1,‡</sup>, J. Büscher<sup>1</sup>, I.G. Darby<sup>1</sup>, W. Dexters<sup>1</sup>,  
D.V. Fedorov<sup>4</sup>, V.N. Fedosseev<sup>5</sup>, K.T. Flanagan<sup>6,7</sup>,  
S. Franchoo<sup>8</sup>, G. Huber<sup>9</sup>, M. Huyse<sup>1</sup>, M. Keupers<sup>1</sup>,  
U. Köster<sup>10</sup>, Yu. Kudryavtsev<sup>1</sup>, E. Mané<sup>7,§</sup>, B.A. Marsh<sup>5</sup>,  
P. Molkanov<sup>4</sup>, R.D. Page<sup>11</sup>, M.D. Seliverstov<sup>1,4,9</sup>,  
A.M. Sjoedin<sup>5,12</sup>, I. Stefan<sup>8</sup>, J. Van de Walle<sup>1,13||</sup>, P. Van  
Duppen<sup>1</sup>, M. Venhart<sup>1,14</sup>, S. Zemlyanoy<sup>15</sup>

<sup>1</sup> Instituut voor Kern- en Stralingsfysica, K.U. Leuven, B-3001 Leuven, Belgium

<sup>2</sup> School of Engineering and Science, University of West Scotland, Paisley, PA1 2BE, United Kingdom

<sup>3</sup> Department of Physics and Biophysics, Comenius University, Bratislava 84248, Slovakia

<sup>4</sup> Petersburg Nuclear Physics Institute, 188350 Gatchina, Russia

<sup>5</sup> Engineering Department, CERN, CH-1211 Geneva 23, Switzerland

<sup>6</sup> Centre de Spectrométrie Nucléaire et de Spectrométrie de Masse, F-91405 Orsay, France

<sup>7</sup> Department of Physics, University of Manchester, Manchester, M60 1AD, United Kingdom

<sup>8</sup> Institut de Physique Nucléaire d'Orsay, F-91406 Orsay, France

<sup>9</sup> Institut für Physik, Johannes Gutenberg Universität, D-55099 Mainz, Germany

<sup>10</sup> Institut Laue-Langevin, F-38042 Grenoble, France

<sup>11</sup> Oliver Lodge Laboratory, University of Liverpool, Liverpool, L69 7ZE, United Kingdom

<sup>12</sup> KTH-Royal Institute of Technology, SE-10044 Stockholm, Sweden

<sup>13</sup> ISOLDE, CERN, CH-1211 Geneva 23, Switzerland

<sup>14</sup> Institute of Physics, Slovak Academy of Sciences, Bratislava 845 11, Slovakia

<sup>15</sup> Joint Institute of Nuclear Research, 141980 Dubna, Moscow Region, Russia

**Abstract.** Complementary studies of  $^{191}\text{Pb}$  have been made in the  $\beta$  decay of  $^{191}\text{Bi}$  at LISOL (CRC) and in the  $\alpha$  decay of  $^{195}\text{Po}$  at ISOLDE (CERN). Fine structures in the  $\alpha$  decay of the low-spin and high-spin isomers of  $^{195}\text{Po}$  have been fully resolved. Identification of the parent state is made possible via isomer selection based on narrow-band laser frequency scanning. The  $\alpha$ -particle and  $\gamma$ -ray energies have been determined with greater precision. New  $\alpha$ -particle and  $\gamma$ -ray energies are identified. Branching ratios in the decay of  $^{195}\text{Po}$  and  $^{191}\text{Pb}$  have been examined.

‡ Present address: GANIL, France

§ Present address: TRIUMF, Canada

|| Present address: KVI, The Netherlands

PACS numbers: 23.20.Nx Internal conversion, 23.60.+e  $\alpha$  decay, 27.80.+w  $190 \leq A \leq 219$ , 29.38.-c Radioactive beams, 32.10.Fn Fine and hyperfine structure

## 1. Introduction

Shape coexistence is an important phenomenon in the region of neutron-deficient lead isotopes and extensive experimental and theoretical studies have been performed [1, 2, 3, 4, 5, 6, 7, 8, 9, 10, 11, 12, 13, 14, 15]. With 109 neutrons,  $^{191}\text{Pb}$  is located in the heart of this region. In the present study, we report on the  $\alpha$  decay of  $^{195}\text{Po}$  and on the  $\beta$  decay of  $^{191}\text{Bi}$ , both parents of  $^{191}\text{Pb}$ . The fine structure in the  $\alpha$  decay of the low-spin isomer  $^{195}\text{Po}^{ls}$  and high-spin isomer  $^{195}\text{Po}^{hs}$  has already been studied in an earlier experiment using the gas-filled separator RITU [7]. An intruder state was identified at 597 keV, suggested as possibly originating from shape coexistence. However, limitations in the production mechanism and measuring conditions prevented determining the conversion coefficient of the decay from that level. The observation of an  $E0$  component in this decay would indicate that the two connected states are of the same spin and parity.

The ground-state and isomer properties of the polonium isotopes have been studied in a campaign of experiments at CERN ISOLDE (Run I in 2007 for  $^{193-200,202,204}\text{Po}$  and Run II in 2009 for  $^{191-192,195,196,201,203,206-211,216,218}\text{Po}$ ) using in-source laser spectroscopy, in an approach similar to that followed for the neutron-deficient lead isotopes [16, 17]. This study allowed the fine structure in the  $\alpha$  decay of  $^{195}\text{Po}$  to be revisited. The relevant parts of the decay chain at mass 195 are shown in Fig. 1.

In a set of complementary experiments, the  $\beta$  decay of the neutron-deficient  $^{191,193}\text{Bi}$  isotopes has been studied at the LISOL facility (CRC, Louvain-La-Neuve, Belgium) as part of a wider survey of the neutron-deficient bismuth isotopes [18, 19, 20, 21, 22]. Comparing the results from the two decay studies gives insight in the determination of the spin of several energy levels in  $^{191}\text{Pb}$ .

## 2. Fine structure $\alpha$ decay of $^{195}\text{Po}$ at ISOLDE and evidence for shape coexistence in $^{191}\text{Pb}$

### 2.1. Experimental procedure

The proton beam from the CERN PS-Booster (1.4 GeV, 1.4  $\mu\text{A}$  on average) impinged upon a  $\text{UC}_x$  target ( $50\text{ g}\cdot\text{cm}^{-2}$ ). The proton pulses were separated by an integer number of periods of 1.2 s in a sequence referred to as the supercycle. Nuclei produced in the spallation reaction diffused out of the target matrix and effused to the high-temperature ( $\approx 2300\text{ K}$ ) RILIS ion source cavity. The atoms were then irradiated with three different laser beams to excite the outer electron resonantly from the polonium atom beyond its ionisation potential and thus create a  $\text{Po}^+$  ion [23]. The ions were then extracted from the ion source cavity, accelerated by DC electrical fields to an energy of 50 keV and mass separated in the dipole magnet of the ISOLDE General Purpose Separator. Note that elements with a low enough ionisation potential, such as thallium, may also be surface ionised. Isobaric contaminants may therefore be present in the mass-separated beam. Yields of a few ten thousands ions per second were delivered for both  $^{195}\text{Po}^{ls}$  and

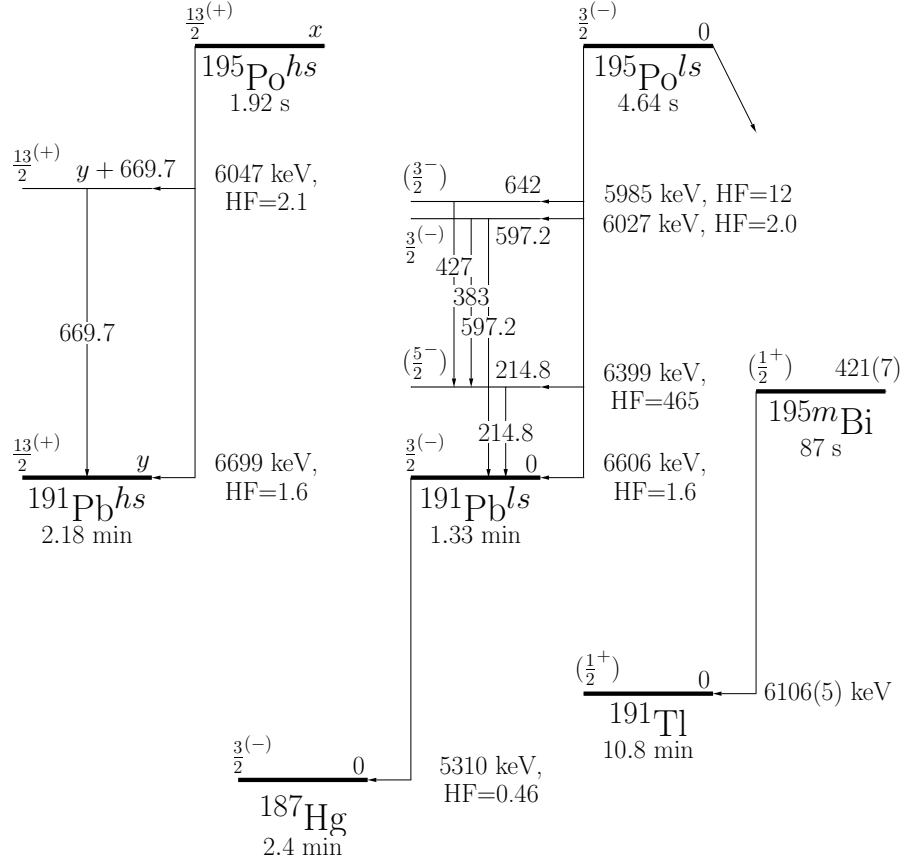


**Figure 1.** Relevant decay schemes of  $^{195}\text{Po}^{hs}$  and  $^{195}\text{Po}^{ls}$  from Ref. [7] and this work. Note that the order and energy difference  $x$  and  $y$  between the low- and high-spin isomers in respectively  $^{195}\text{Po}$  and  $^{191}\text{Pb}$  are not known.

$^{195}\text{Po}^{hs}$  isomers, consistent with those published in Ref. [23].

The ions were implanted in one of ten carbon foils ( $20 \mu\text{g}\cdot\text{cm}^{-2}$ ) mounted on a rotating wheel. In Run I, a single Si detector (active area  $150 \text{ mm}^2$ , thickness  $300 \mu\text{m}$ ) was mounted behind the foil at the implantation position. During Run II, that same position was surrounded by two Si detectors, a circular detector behind the foil (back detector, active area  $300 \text{ mm}^2$ , thickness  $300 \mu\text{m}$ ) and an annular detector in front of the foil (front detector, active area  $450 \text{ mm}^2$ , thickness  $300 \mu\text{m}$ ) that let the ion beam pass through. The total solid angle coverage was improved from 33% to 66% of  $4\pi$ . The Full Width at Half Maximum (FWHM) energy resolution of those detectors for  $\alpha$  particles with  $E_\alpha = 5.5 \text{ MeV}$  was 25 keV, 20 keV and 30 keV, respectively. A coaxial HPGe detector was placed behind the back Si detector outside the vacuum chamber for Run II. Its energy resolution (FWHM) was 4.3 keV at  $E_\gamma = 1.3 \text{ MeV}$ . The wheel was rotated synchronously with every second PS-Booster supercycle to remove the relatively long-lived bismuth and lead daughter activities.

The  $\alpha$ -particle energy spectra are shown in Fig. 2, in which only  $\alpha$  particles emitted

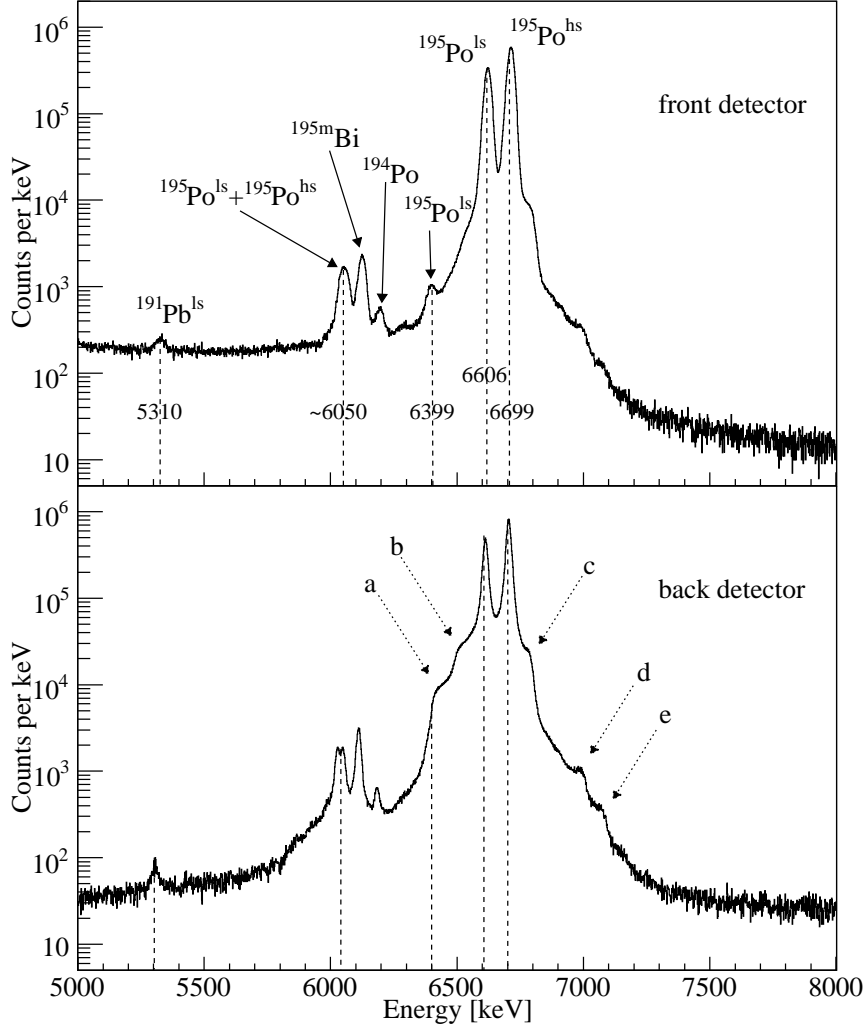


**Figure 2.**  $\alpha$ -particle energy spectra measured at mass number 195 while ionising polonium (Run II) using the front detector (top) and the back detector (bottom) over a period of 4 hours. The peaks are labelled in the top spectrum with their assignments. The low- and high-energy tails of the two main  $\alpha$  lines, indicated by dotted arrows in the bottom spectrum, are labelled for the discussion in the text.

in the decay of  $^{195}\text{Po}$  and of the daughters  $^{191}\text{Pb}$  (after  $\alpha$  decay) and  $^{195m}\text{Bi}$  (after  $\beta^+/\text{EC}$  decay) can be seen. The  $^{194}\text{Po}$  peak in the spectrum originates from mass contamination of  $A = 194$  in  $A = 195$  due to the tail of the mass line of that isotope. No  $^{195}\text{Tl}$  contribution can be directly observed in this spectrum as it is a pure  $\beta^+/\text{EC}$ -decaying isotope. A very intense  $\gamma$ -ray transition at 384 keV, coming from the internal decay of  $^{195m}\text{Tl}$  [24], is however observed in the  $\gamma$ -ray energy spectrum shown in Fig. 3.

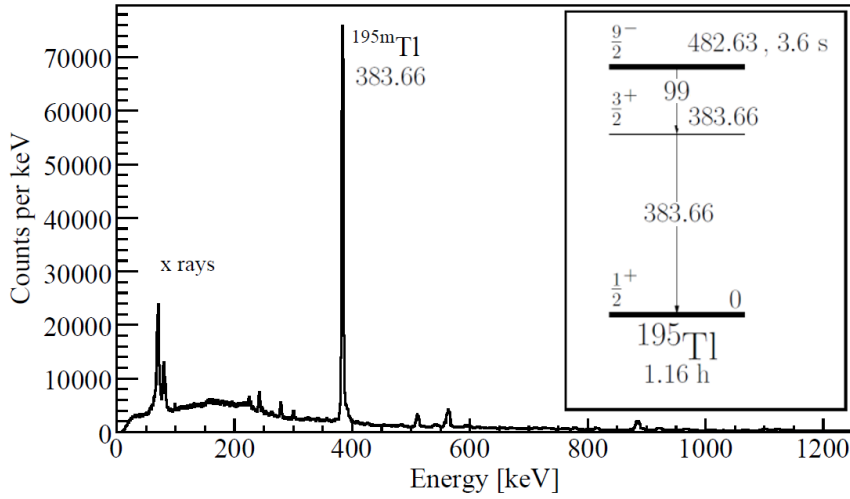


**Figure 3.**  $\gamma$ -ray energy spectrum measured at mass number 195 while ionising polonium (Run II), in coincidence with any decay event in the Si detectors. The  $\gamma$  rays that are not labelled are all attributed to the  $\beta$  decay of  $^{195g}\text{Tl}$ . Inset: decay scheme of  $^{195m}\text{Tl}$  [24].

## 2.2. Features of the $\alpha$ spectra

Several features are observed in the  $\alpha$ -particle energy spectra in Fig. 2, in addition to the main peaks. Let's consider first the low-energy tails observed on the  $\alpha$  peaks, which are most visible on the two main transitions at  $E_\alpha = 6606$  keV and  $E_\alpha = 6699$  keV. These two tails are labelled *a* and *b* in the second spectrum and can be explained by the energy loss of the  $\alpha$  particles emitted through the carbon foil. Calculations indicate that at a beam energy of 50 keV, the polonium isotopes are implanted at a depth of 25 nm [25] compared to the 90 nm thickness of the foil. This tail has a cut-off due to the limited angular range covered by the detectors and allowed by the foil mount geometry, and is more pronounced in the back detector.

A high-energy tail is also present and is attributed to the random summing of the energy of an  $\alpha$  particle from the decay of  $^{195}\text{Po}$  with that of a positron from the  $\beta$  decay of  $^{195}\text{Tl}$ . The maximum  $\beta$  summing for the two main peaks in Fig. 2, corresponding to the energy loss of a  $\beta$  particle in a Si detector, is indicated by *d* and *e*.

Another feature of the  $\alpha$ -particle energy spectrum, labelled *c* in Fig. 2, is a broad shoulder on top of the high-energy tail from  $\beta$  summing. This extra shoulder has been identified through  $\alpha$ - $\gamma$  coincidences. Fig. 4 shows the energy of the  $\alpha$  particles as a function of the  $\alpha$ - $\gamma$  time difference  $\Delta t$  for events in coincidence with the 384 keV  $\gamma$ -ray transition from the internal decay of  $^{195m}\text{Tl}$  (see inset in Fig. 3). The two broad bands at an  $\alpha$  energy of 6606 keV and 6699 keV are due to random coincidences with the 384 keV transition. Both bands exhibit a side structure that seems to vanish at  $\Delta t \approx 1200$  ns. This is attributable to the true coincidence between the 384 keV  $\gamma$  ray and the

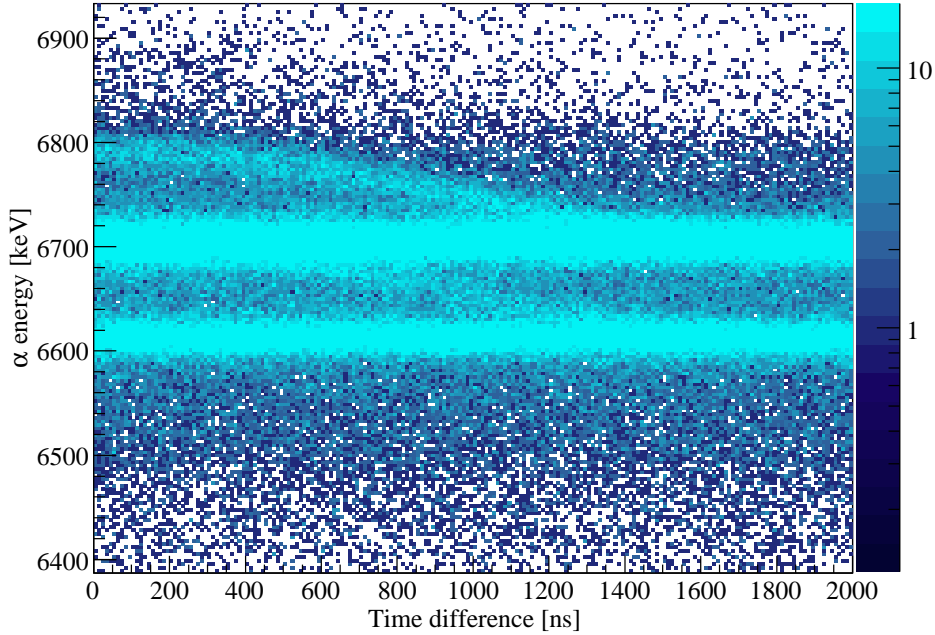


**Figure 4.** (Color online) Energy of the  $\alpha$  particles as a function of the  $\alpha$ - $\gamma$  time difference  $\Delta t$  for events in coincidence with the  $\gamma$ -ray transition at 384 keV from the internal decay of  $^{195m}\text{Tl}$  (Run II). The  $y$  axis shows the energy recorded in the Si detector while the  $x$  axis shows the time difference between the Si detector and the Ge detector.

strongly-converted ( $\alpha_{tot} = 161$  [26]) transition at 99 keV in the decay of  $^{195m}\text{Tl}$ . The energy of the electron emitted by the latter sums with the energy of the  $\alpha$  particles randomly. The observed time dependence of the side structure is due to the integration time of the amplifier. For this setup, complete integration is achieved in 1000 ns, beyond which partial summing occurs.

### 2.3. Fine-structure $\alpha$ decay and branching ratio determination

The fine-structure decays of  $^{195}\text{Po}$  have been investigated using the  $\alpha$ - $\gamma$  coincidence data. The  $\gamma$ -ray energy spectra in prompt coincidence with the  $\alpha$ -decay peaks of  $^{195}\text{Po}^{ls,hs}$  identified around  $E_\alpha = 6000$  keV and  $E_\alpha = 6400$  keV are shown in Fig. 5. Two previously observed transitions at 597.2(5) keV and 669.6(5) keV [7] can be seen. Additional transitions at 143(1), 214.8(5), 383(1), 427(1) and 483(1) keV are identified for the first time. The energy of the transitions at 214.8 and 383 keV add up to 597.8(12) keV and are therefore consistent with a cascade that decays from the 597.2 keV level.

The energy of the  $\alpha$  particles populating each state can be determined by gating on the  $\gamma$ -ray transitions separately to produce  $\gamma$ -gated  $\alpha$ -particle energy spectra, shown in Fig. 6. The two known  $\alpha$  decays around 6050 keV can be cleanly identified as (1) an  $\alpha$  decay with energy  $E_\alpha = 6047(5)$  keV in coincidence with the 669.6 keV  $\gamma$ -ray



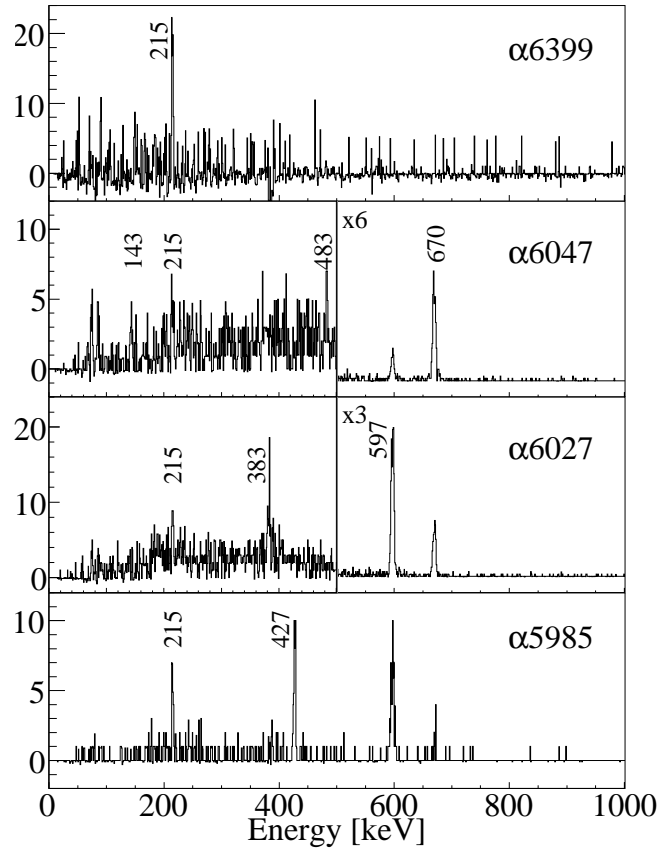


**Figure 5.** From top to bottom: background- and random-subtracted  $\gamma$ -ray energy spectra in coincidence with the  $\alpha$  particles with energy around 6399 keV (top), 6047 keV, 6027 keV or 5985 keV (bottom) from the fine structures in the decay of  $^{195}\text{Po}$  (Run II). The  $\gamma$  rays are labelled according to their energy in keV.

transition and (2) an  $\alpha$  decay with energy  $E_\alpha = 6027(5)$  keV in coincidence with the 597.2 keV  $\gamma$ -ray transition. This 6027 keV  $\alpha$  decay is also observed in coincidence with the 383 keV and 214.8 keV  $\gamma$ -ray transitions. Also in coincidence with the 214.8 keV  $\gamma$ -ray transition are  $\alpha$  decays at energies 5985(10) keV, 6047 keV and 6399(10) keV. The  $\alpha$  particles at energy 5985 and 6399 keV are observed for the first time in the  $\alpha$  decay of  $^{195}\text{Po}$ . In the spectrum of the 427 keV  $\gamma$  transition, the new  $\alpha$ -decay peak at an energy of 5985 keV is also observed and suggests therefore a second cascade with the transitions at 214.8 and 427 keV. The new energy level populated by this  $\alpha$  decay is then at 642(1) keV. The presence of the 6047 keV  $\alpha$ -decay peak in coincidence with the 214.8 keV transition shows that there is a possible connection between the high-spin and the low-spin structures. The two  $\gamma$  rays with energy 143 keV and 483 keV, showing a coincidence with the fine-structure  $\alpha$ -decay at 6047 keV from the decay of the high-spin isomer  $^{195}\text{Po}^{hs}$ , are possible candidates for this connection. However, since no  $\gamma - \gamma$  coincidences are available, those transitions remain unplaced in the level scheme

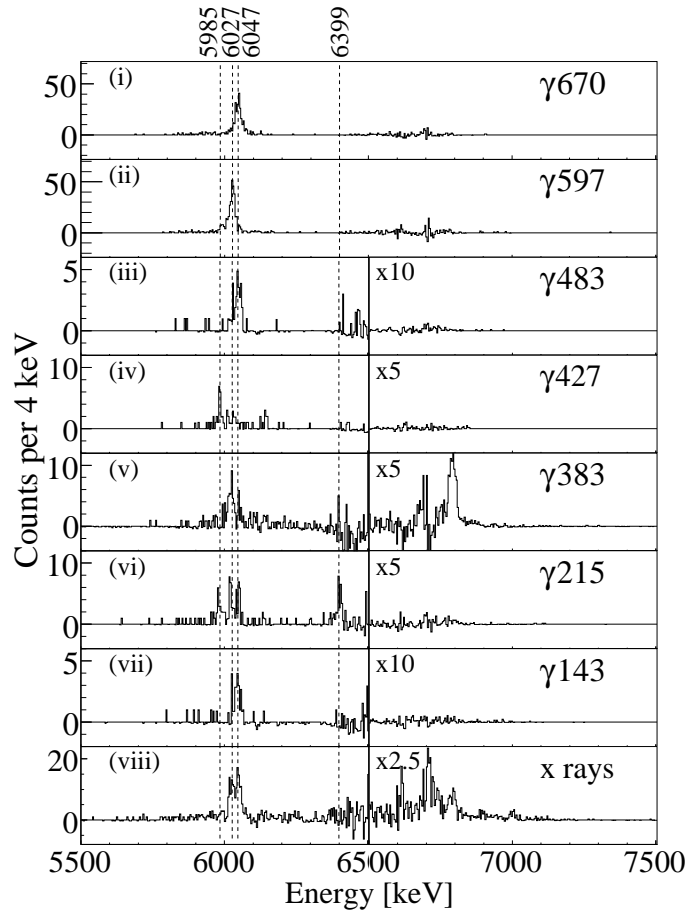


**Figure 6.** (i-viii) Background- and random-subtracted  $\gamma$ -gated  $\alpha$ -particle energy spectra (Run II). The  $\alpha$ -particle energies are labelled in keV. The intensity fluctuations around 6.6-6.7 MeV arise from the very intense  $\alpha$  decays at 6606 and 6699 keV and do not represent true  $\alpha$ - $\gamma$  coincidences. (v) The summed  $\alpha$ -electron energies are observed due to the proximity of the 384 keV  $\gamma$ -ray from the internal decay of  $^{195m}\text{Tl}$ . (viii) Similarly, the highly-converted 99 keV transition from the internal decay of  $^{195m}\text{Tl}$  results in coincidences between x rays and the summed  $\alpha$ -electron events.

of  $^{191}\text{Pb}$ .

The assignment of the different components to the decay of the low- or high-spin isomer of  $^{195}\text{Po}$  has been discussed in Ref. [7] in terms of the  $Q_\alpha$  value, from which it was concluded that the 6027 – 597.2 keV decay comes from the low-spin  $^{195}\text{Po}^{ls}$  isomer while the 6047 – 669.6 keV decay comes from the high-spin  $^{195}\text{Po}^{hs}$  isomer. The same technique confirms that the new decays 5985 – 427 – 214.8 keV and 6399 – 214.8 keV arise from the decay of the low-spin  $^{195}\text{Po}^{ls}$  isomer.

Using the different atomic hyperfine profiles of the two nuclear states in  $^{195}\text{Po}$ , it is also possible to enhance the production of one of the isomers over the other. The use of such isomeric beams has already been demonstrated for other elements [27]. The hyperfine spectra for both nuclear states using the second transition of the ionisation scheme at 843.38 nm, as described in Ref. [23], is shown in Fig. 7. The regions enhancing

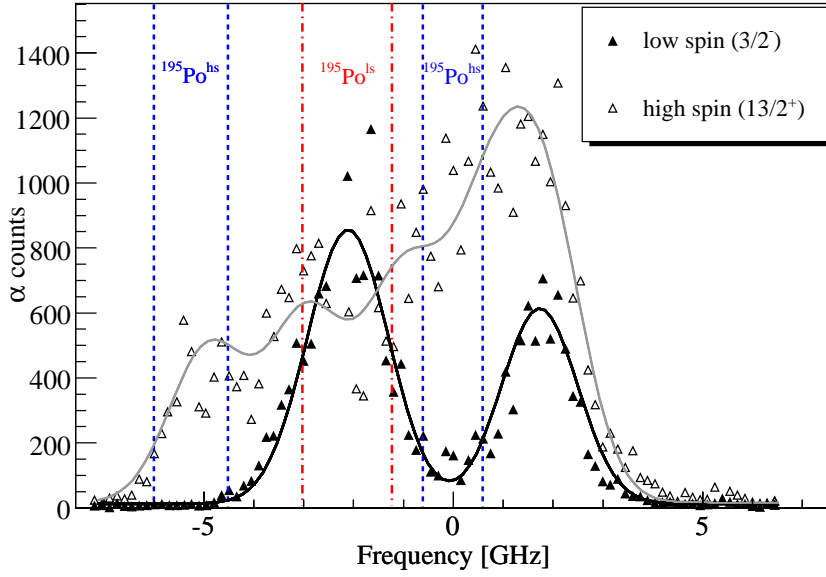


**Figure 7.** (Color online) Hyperfine structure of  $^{195}\text{Po}^{ls}$  (full triangles, black line) and  $^{195}\text{Po}^{hs}$  (open triangles, grey line) using the atomic transition at 843.38 nm from the ionisation scheme of polonium (Run I). The range used to study  $^{195}\text{Po}^{ls}$  is limited by the red dot-dashed lines while those for  $^{195}\text{Po}^{hs}$  are limited by the blue dashed lines. The background (off-resonance) range is taken on the far right (Frequency > 4.5 GHz) of the spectrum.

the production of each isomer with respect to the other are highlighted. The background-subtracted  $\alpha$ -particle energy spectra for each laser frequency range are selectively combined to create isomerically-pure  $\alpha$ -particle energy spectra, shown in Fig. 8. The fine-structure  $\alpha$  particles can then be unambiguously assigned to the decay of one or the other isomer of  $^{195}\text{Po}$ . Note however that other isotopes of polonium can be identified in those spectra due to the poorer mass resolution in Run I (as compared to Run II) and to their dependence on the laser frequency. The transitions, their assignments, energies and relative intensities are summarised in Table 1.

Combining the relative intensities with the partial information available in Ref. [7], we can extract the conversion coefficient of the transition at 597.2 keV in two ways. First, the relative intensity of the 6027 keV  $\alpha$ -decay of  $^{195}\text{Po}^{ls}$ ,  $I_\alpha = 0.34(3)\%$ , measured in this study, can be compared with the known contribution from the  $\alpha$ - $\gamma$  chain,  $I_{\alpha\gamma} = 0.17(5)\%$ , given in Ref. [7], yielding a conversion coefficient  $\alpha = 0.9(6)$ . Alternatively, we can rescale the known value of  $\alpha = 0.8(3)$  for the 669.6 keV transition in  $^{191}\text{Pb}^{hs}$  from Ref. [7] by comparing the  $\alpha$  branching ratios and  $\gamma$  intensities in the decay of  $^{195}\text{Po}^{ls,hs}$ , yielding a value of  $\alpha = 0.5(3)$ . In both cases, the influence of the 382.8 keV transition from that level is also taken into account. Note that the coincidence between the  $\alpha$  decays at 6027 keV and 6047 keV with the lead x rays

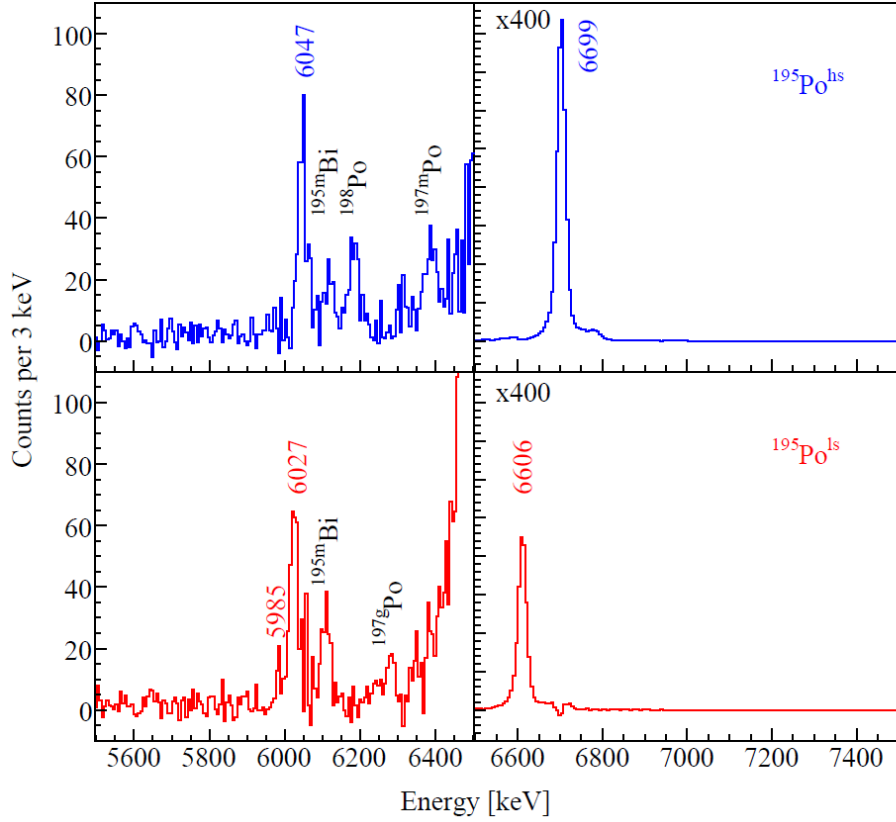


**Figure 8.** (Color online) Background-subtracted isomerically-purified  $\alpha$ -particle energy spectra of  $^{195}\text{Po}^{ls}$  (red-bottom) and  $^{195}\text{Po}^{hs}$  (blue-top) using the ranges indicated in Fig. 7 (Run I). The  $\alpha$ -decay peaks from  $^{195}\text{Po}$  are labelled according to their energy in keV while the peaks not directly associated with the decay of  $^{195}\text{Po}$  are labelled according to the decaying isotope. The  $\alpha$  particle with energy 6399 keV cannot be seen in this spectrum because it lies under the low-energy tail of the more intense 6606 keV  $\alpha$ -particle energy peak.

**Table 1.** Properties of the fine-structure decays of  $^{195}\text{Po}^{ls}$  and  $^{195}\text{Po}^{hs}$ :  $\alpha$ -particle energy  $E_\alpha$  and relative intensity  $I_\alpha$ , Hindrance Factor with respect to the ground-state-to-ground-state  $\alpha$  decay of the neighbouring even- $A$  nuclei HF, energy of the excited state in the daughter nucleus  $E^*$  and conversion coefficient  $\alpha$  of the direct decay of that excited level to the isomer in  $^{195}\text{Po}$ .

Isotope	$E_\alpha$ [keV]	$I_\alpha$ [%]	HF	$E^*$ [keV]	$\alpha$
$^{195}\text{Po}^{ls}$	6606(5) [28]	99.56(2)	1.6(1)	0	
	6399(10)	0.054(12)	465(114)	214.8(5)	
	6027(5)	0.34(3)	2.0(2)	597.2(5)	0.6(3)
	5985(10)	0.036(3)	12(2)	642(1)	
$^{195}\text{Po}^{hs}$	6699(5) [28]	99.83(1)	1.6(1)	0	
	6047(5)	0.17(1)	2.1(2)	669.6(5)	0.8(3) [7]

**Table 2.** Branching ratios in the decay of  $^{195}\text{Po}^{ls}$  and  $^{191}\text{Pb}^{ls}$  from this work and the literature.

Isotope	$b_\alpha$ [%]	$b_\alpha^{lit}$ [%]
$^{195}\text{Po}^{ls}$	94(4)	63(25) [28]
$^{191}\text{Pb}^{ls}$	0.051(5)	0.013(5) [30]

(Fig. 6 viii) confirms that the transitions at 597.2 and 669.6 keV have a significant conversion coefficient. From the weighted average between those two independent estimates, a conversion coefficient of 0.6(3) is found compared to the calculated values  $\alpha_{tot}(E2) = 0.019$ ,  $\alpha_{tot}(M1) = 0.068$  and  $\alpha_{tot}(E1) = 0.007$ . From this we conclude that the 597.2 keV transition has a large  $E0$  contribution, confirming the matching spin and parity assignments for the low-spin isomer and the 597.2 keV level in  $^{191}\text{Pb}$ . Based on the spin assignment, this level is a good candidate for a state with a different shape than the low-spin isomer, as suggested in Ref. [7]. Moreover, such a large  $E0$  component to its decay is only possible if the two connected levels have similar configurations and indicates that the two shape-coexisting states are also considerably mixed [2]. A quantitative determination of the amount of mixing cannot be based on this result alone and requires additional experimental information (e.g. the excited state lifetime).

We now consider the  $\alpha$ -decay branching ratios of  $^{195}\text{Po}^{ls}$  and  $^{191}\text{Pb}^{ls}$ . Accounting for the different lifetimes and the fraction of the implants that recoil out of the carbon foil after emitting an  $\alpha$  particle [29], accurate branching ratios for the low-spin states can be extracted. The  $\alpha$  branching ratio for  $^{191}\text{Pb}^{ls}$  is found to be  $b_\alpha = 0.051(5)\%$ . The beta-decay branch of  $^{195}\text{Po}^{ls}$  can be estimated by looking at the  $\alpha$  decay of its daughter nucleus  $^{195m}\text{Bi}$ . Although the precision on its branching ratios is limited [19], the fraction of  $^{195}\text{Po}^{ls}$  that  $\beta$ -decays is small enough that a good accuracy for the  $b_\alpha(^{195}\text{Po})$  may still be achieved. A value of  $b_\alpha = 94(4)\%$  is found, assuming that the  $\beta$  decay of  $^{195}\text{Po}^{ls}$  only populates the  $I = (\frac{1}{2}^+)$  state in  $^{195}\text{Bi}$ . Those values are consistent with the previous literature values [28, 30], as shown in Table 2, but are more precise thanks to larger statistics. No new branching ratios could be determined in the decay of  $^{195}\text{Po}^{hs}$  or  $^{191}\text{Pb}^{hs}$  as the  $\alpha$  decays of the high-spin  $^{195}\text{Bi}$  and  $^{191}\text{Pb}^{hs}$  are not observed.

Using the formalism of Rasmussen [31], Hindrance Factors (HF) in the decay of  $^{195}\text{Po}$  with respect to  $^{194,196}\text{Po}$  [28], assuming no change in angular momentum ( $\Delta l = 0$ ), are calculated and given in Table 1. Most of the HF values in the main component and in the fine structure decay of  $^{195}\text{Po}^{ls}$  and  $^{195}\text{Po}^{hs}$  are low (1–3). This means that those  $\alpha$  decays are unhindered and that the spin and parity of the mother and daughter states are the same. The conclusions presented in Ref. [7] are thus all confirmed. The high HF value (465(114)) of the 6399 keV  $\alpha$  decay, however, indicates a change in spin or configuration between  $^{195}\text{Po}^{ls}$  and the 214.8 keV excited level in  $^{191}\text{Pb}^{ls}$ . In the case of the 5985 keV  $\alpha$  decay, the slightly higher HF value (12(2)) points to a different nature of the 642 keV level in  $^{191}\text{Pb}^{ls}$  compared to the  $^{195}\text{Po}^{ls}$  isomer but nonetheless with

a likely spin assignment ( $\frac{3}{2}^-$ ). Finally, the HF in the decay of  $^{191}\text{Pb}^{ls}$  with respect to  $^{190,192}\text{Pb}$  [32] shows also a small value of 0.46(7), consistent with an unhindered decay to the  $I^\pi = \frac{3}{2}^{(-)}$  isomer  $^{187m}\text{Hg}$  [33]. This offers an experimental confirmation, according to the  $\Delta l = 0$   $\alpha$ -decay strong rule, that the spin assignment of the  $^{191}\text{Pb}^{ls}$  isomer is indeed  $I^\pi = \frac{3}{2}^{(-)}$ , and thus similarly for the excited state at 597.2 keV and for the  $^{195}\text{Po}^{ls}$  isomer. Similarly, by combining the spin assignment  $\frac{13}{2}^{(+)}$  in  $^{191}\text{Pb}^{hs}$  [34] with the identification of an  $E0$  component in the decay of the 669.6 keV level [7], a spin assignment  $\frac{13}{2}^{(+)}$  is confirmed for that excited state. The spin assignment  $\frac{13}{2}^{(+)}$  of the high-spin  $^{195}\text{Po}^{hs}$  isomer is also confirmed through the low HF (1.6(1)/2.1(1)).

### 3. $\beta$ decay of $^{191,193}\text{Bi}$ in LISOL and migration of the $\nu 2f_{5/2}$ single-particle energy level in neutron-deficient lead isotopes

The  $\alpha$  and  $\beta$  decays of the neutron-deficient  $^{192-196}\text{Bi}$  isotopes were studied at the LISOL facility (CRC, Louvain-La-Neuve, Belgium) in the 1980s [18, 19, 20, 21, 22]. The radioactive nuclei were produced in fusion-evaporation reactions using  $^{14}\text{N}$ ,  $^{16}\text{O}$  and  $^{20}\text{Ne}$  beams on natural Ir (37.3%  $^{191}\text{Ir}$ , 62.7%  $^{193}\text{Ir}$ ), natural Re (37.4%  $^{185}\text{Re}$ , 62.6%  $^{187}\text{Re}$ ) and  $^{181}\text{Ta}$  targets, respectively. The radioactive recoils were subsequently ionised in a plasma ion source, mass separated and implanted in an aluminised mylar tape. Single  $\gamma$ -ray energy spectra were recorded with two coaxial HPGe detectors.

The lists of observed  $\gamma$ -ray energies in the  $\beta$  decay of  $^{191,193}\text{Bi}$  are given in Tables 3 and 4. For  $^{193}\text{Bi}$ , relative efficiencies  $I_\gamma$  are also given. By matching the summed energies of several  $\gamma$ -ray transitions with observed  $\gamma$ -ray energies, possible cross-over transitions in the decay of some excited levels are proposed. Note that true summing in the  $\gamma$  detectors alone cannot explain the observed relative intensities and that those transitions are therefore real.

From the study of the decay of the isotopes  $^{195,197}\text{Bi}$  [21, 22], it has been observed that the most intense transition leading to the low-spin isomer in the lead daughter isotope is the decay of the  $\frac{5}{2}^-$  excited state to the  $\frac{3}{2}^-$  state and was interpreted as the transition between the  $\nu 2f_{5/2}$  and  $\nu 3p_{3/2}$  quasiparticle states. By comparing the relative intensities of the different transitions presented in Table 4, the 174.5 keV level in  $^{193}\text{Pb}$  is therefore a good candidate for a similar configuration, dominated by a quasiparticle excitation in the  $\nu 2f_{5/2}$  level. In the case of  $^{197}\text{Pb}$  [22], a calculation using a surface delta interaction [35] concluded that these levels had actually almost 100% one-quasiparticle character. A similar behaviour might be expected for  $^{193}\text{Pb}$ .

In  $^{191}\text{Pb}$ , the 214.8 keV level is populated both by the  $\beta$  decay of the high-spin  $I^\pi = (\frac{9}{2}^-)$  state in  $^{191}\text{Bi}$  isotope and in the  $\alpha$  decay of the low-spin  $I^\pi = \frac{3}{2}^{(-)}$  state in  $^{195}\text{Po}^{ls}$  isotope. Considering the high HF in the  $\alpha$  decay, only spin assignments of  $I = \frac{5}{2}$  or  $\frac{7}{2}$  are possible. Based on the systematics of the low-excitation energy levels in the neighbouring odd- $A$  Pb isotopes, a spin assignment ( $\frac{5}{2}^-$ ) is proposed, corresponding similarly as before to a mostly one-quasiparticle  $\nu 2f_{5/2}$  level. The systematics of the lowest energy levels with spin  $\frac{1}{2}^-$ ,  $\frac{3}{2}^-$ ,  $\frac{5}{2}^-$ , and  $\frac{13}{2}^+$  are shown in Fig. 9. Since no data

**Table 3.** List of  $\gamma$ -ray energies  $E_\gamma$  and relative intensities  $I_\gamma^{ls,hs}$  in the  $\alpha$  decay of  $^{195}\text{Po}^{ls,hs}$ , respectively, observed in the excited structure of  $^{191}\text{Pb}$  from the  $\alpha$  decay of  $^{195}\text{Po}$  and the  $\beta$  decay of  $^{191}\text{Bi}$ .

Isotope	$E_\gamma$ [keV]	$I_\gamma^{ls}$ [%]	$I_\gamma^{hs}$ [%]	Origin	Coincident $\gamma$ -ray
$^{191}\text{Pb}$	143(1)		3.5(10)	$\alpha, \beta$	
	214.8(5)			$\alpha, \beta$	383, 427
	383(1)	9(2)		$\alpha$	214.8
	427(1)	7(2)		$\alpha$	214.8
	483(1)		13(3)	$\alpha$	
	597.2(5)	100		$\alpha$	
	669.6(5)		100	$\alpha, \beta$	
	708.26			$\beta$	
	820.2			$\beta$	
	954.7			$\beta$	
	1082.3			$\beta$	
	1117.71			$\beta$	

can yet assert for the purity of the wavefunctions of these levels far from stability, the single-particle energy levels cannot be directly deduced from these systematics. Note however that they mostly arise from a single neutron particle or hole in the  $\nu 3p_{1/2}$ ,  $\nu 3p_{3/2}$ ,  $\nu 2f_{5/2}$  and  $\nu 1i_{13/2}$  orbitals.

#### 4. Conclusion

In conclusion, using resonant laser ionisation, a new study of the  $\alpha$  decay of  $^{195}\text{Po}$  was made.  $\alpha$ -particle and  $\gamma$ -ray energies in the  $\alpha$  decay of the low-spin and high-spin isomers, branching ratios and a conversion coefficient have been extracted with better precision. Hindrance Factor values for the  $\alpha$  decay confirm the spin assignments  $I^\pi = \frac{3}{2}^{(-)}$  for the low-spin isomers  $^{191}\text{Pb}^{ls}$  and  $^{195}\text{Po}^{ls}$ . Using the fine structure decay of  $^{195}\text{Po}^{ls}$ , the conversion coefficient for the decay of the 597.2 keV energy level to the lowest energy state in  $^{191}\text{Pb}^{ls}$  is measured for the first time, confirming the spin assignment  $I^\pi = \frac{3}{2}^{(-)}$ . The large value of the conversion coefficient confirms the presence of a strong  $E0$  component in the 597.2 keV transition and makes the 597.2 keV  $\frac{3}{2}^{(-)}$  level a good candidate for shape-coexisting state as observed in the neighbouring Pb isotopes. A new level is found at 214.8 keV and is also observed in the  $\beta$  decay of  $^{191}\text{Bi}$ , allowing a spin assignment of  $I^\pi = (\frac{5}{2}^-)$ . It is a good candidate for the one-quasiparticle excitations  $\nu 2f_{5/2}$  level and extends the systematics of low-lying energy levels in the neutron-deficient lead isotopes down to  $^{191}\text{Pb}$ . Finally, a new level is also found at 642 keV. A tentative spin assignment  $I^\pi = (\frac{3}{2}^-)$  is proposed based on the evaluated HF.

**Table 4.** List of  $\gamma$ -ray energies  $E_\gamma$  and relative intensities  $I_\gamma$  with respect to the 174.5 keV transition observed in the excited structure of  $^{193}\text{Pb}$  from the  $\beta$  decay of  $^{193}\text{Bi}$ . The proposed cross-over transitions are based on summed  $\gamma$ -ray energies matching an observed  $\gamma$ -ray energy with too large relative intensity to be attributed to summing effects in the detector.

Isotope	$E_\gamma$ [keV]	$I_\gamma$ [%]	Possible cross-over
$^{193}\text{Pb}$	174.5	100	
	196.8	5.4	
	290.6	7.8	
	320.1	7.7	
	354	8.7	
	505.9	5.2	
	554.2	38	
	621.2	9.2	
	681.1	48	
	687.2	12.4	
	711.1	48.8	
	739.1	13.5	
	750.1	6.3	196.8 + 554.2
	818.5	14.2	196.8 + 621.2
	861.8	20	174.5 + 687.6
	873.9	29.4	320.1 + 554.2
	995.7	23.8	
	1022.3	12.8	
	1049.1	9.9	174.5 + 873.9
	1116.1	8.4	
	1124.7	5.2	
	1171.6	10.1	174.5 + 995.7
			354 + 818.5
	1630.6	0.4	505.9 + 1124.7

## Acknowledgments

We would like to thank the ISOLDE collaboration and the CRC team for providing excellent beams, and the GSI Target group for making the carbon foils. This work was supported by FWO-Vlaanderen (Belgium), GOA/2004/03 (BOF-K.U.Leuven), by the IUAP - Belgian State Belgian Science Policy - (BriX network P6/23), by the European Commission within the Sixth Framework Programme through I3-EURONS (Contract RII3-CT-2004-506065), by the U.K. Science and Technology Facilities Council, and by the Slovak grant agency VEGA (Contract No. 1/0091/10).



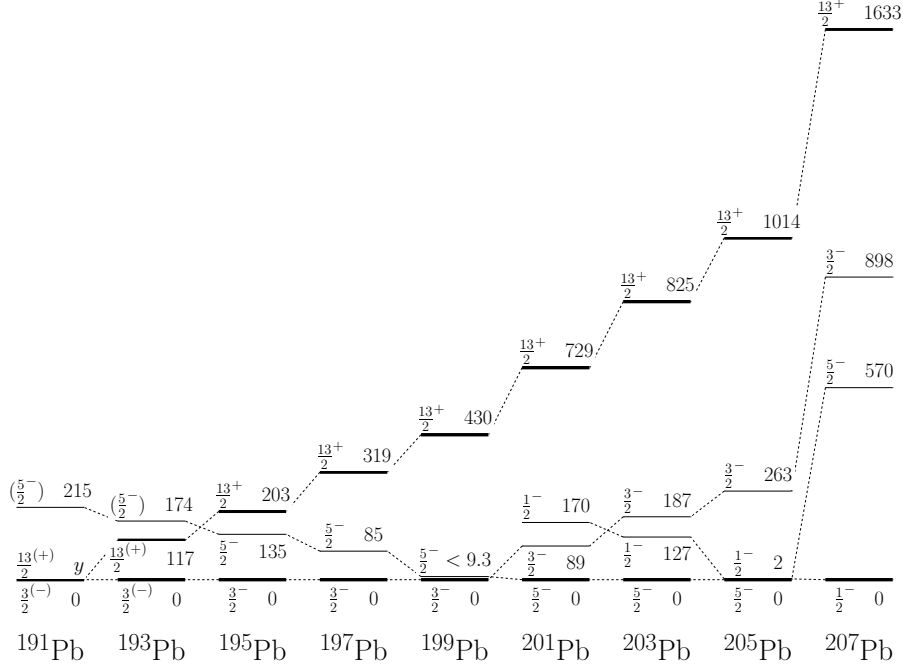


**Figure 9.** Systematics of the lowest-lying energy levels with spin and parity  $\frac{1}{2}^-$ ,  $\frac{3}{2}^-$ ,  $\frac{5}{2}^-$ , and  $\frac{13}{2}^+$  in neutron-deficient odd- $A$  Pb isotopes. These levels are dominated by one-quasiparticle excitations of the  $\nu 3p_{1/2}$ ,  $\nu 3p_{3/2}$ ,  $\nu 2f_{5/2}$ , and  $\nu 1i_{13/2}$  orbitals, respectively. This extends the previous systematics presented in Ref. [21]. Note that the order of the lowest energy states ( $\frac{3}{2}^-$ ,  $\frac{13}{2}^+$ ) in  $^{191}\text{Pb}$  and their relative excitation energy  $y$  are not known.

## References

- [1] K. Heyde, P. Van Isacker, M. Waroquier, J.L. Wood, and R.A. Meyer. Coexistence in odd-mass nuclei. *Phys. Rep.*, 102:291–393, 1983.
- [2] J.L. Wood, K.H. Heyde, W. Nazarewicz, M. Huyse, and P. Van Duppen. Coexistence in even-mass nuclei. *Phys. Rep.*, 215:101–201, 1992.
- [3] A.M. Oros, K.H. Heyde, C. De Coster, B. Decroix, R. Wyss, B. R. Barrette, and P. Navratil. Shape coexistence in the light Po isotopes. *Nucl. Phys. A*, 645:107–142, 1999.
- [4] A.N. Andreyev, M. Huyse, P. Van Duppen, L. Weissman, D. Ackermann, J. Gerl, F.P. Heßberger, S. Hofmann, A. Kleinböhl, G. Münzenberg, S. Reshitko, C. Schlegel, H. Schaffner, P. Cagarda, M. Matos, S. Saro, A. Keenan, C. Moore, C.D. O’Leary, R.D. Page, M. Taylor, H. Kettunen, M. Leino, A. Lavrentiev, R. Wyss, and K.H. Heyde. A triplet of differently shaped spin-zero states in the atomic nucleus  $^{186}\text{Pb}$ . *Nature*, 405:430–433, 2000.
- [5] P. Van Duppen and M. Huyse. Shape coexistence around the  $Z = 82$  closed shell probed by  $\alpha$ -decay. *Hyp. Int.*, 129:149–161, 2000.
- [6] R. Julin, K. Helariutta, and M. Muikku. Intruder states in very neutron-deficient Hg, Pb and Po nuclei. *J. of Phys. G*, 27:R109–R139, 2001.
- [7] K. Van de Vel, A.N. Andreyev, M. Huyse, P. Van Duppen, J.F.C. Cocks, O. Dorvaux, P.T. Greenlees, K. Helariutta, P. Jones, R. Julin, S. Juutinen, H. Kettunen, P. Kuusiniemi, M. Leino, M. Muikku, P. Nieminen, K. Eskola, and R. Wyss. Identification of low-lying proton-based intruder states in  $^{189-193}\text{Pb}$ . *Phys. Rev. C*, 65:064301, 2002.
- [8] A.N. Andreyev, M. Huyse, K. Van de Vel, P. Van Duppen, O. Dorvaux, P. Greenlees, K. Helariutta, P. Jones, R. Julin, S. Juutinen, H. Kettunen, P. Kuusiniemi, M. Leino, M. Muikku, P. Nieminen,

- P. Rahkila, J. Uusitalo, R. Wyss, K. Hauschild, and Y. Le Coz. In-beam  $\alpha$ -decay spectroscopy of  $^{191}\text{Po}$  and evidence for triple shape coexistence at low energy in the daughter nucleus  $^{187}\text{Pb}$ . *Phys. Rev. C*, 66:014313, 2002.
- [9] M. Bender, T. Cornelius, G.A. Lalazissis, J.A. Maruhn, W. Nazarewicz, and Reinhard P.-G. The  $Z = 82$  shell closure in neutron-deficient Pb isotopes. *Eur. Phys. J. A*, 14:23–28, 2002.
- [10] T. Nikšić, D. Vretenar, P. Ring, and G.A. Lalazissis. Shape coexistence in the relativistic Hartree-Bogoliubov approach. *Phys. Rev. C*, 65:054320, 2002.
- [11] K. Van de Vel, A.N. Andreyev, R.D. Page, H. Kettunen, P.T. Greenlees, P. Jones, R. Julin, S. Juutinen, H. Kankaanpää, A. Keenan, P. Kuusiniemi, M. Leino, M. Muikku, P. Nieminen, P. Rahkila, J. Uusitalo, K. Eskola, A. Hürstel, M. Huyse, Y. Le Coz, M. B. Smith, P. Van Duppen, and R. Wyss. Fine structure in the  $\alpha$  decay of  $^{188,192}\text{Po}$ . *Phys. Rev. C*, 68:054311, 2003.
- [12] N. Smirnova, P.-H. Heenen, and G. Neyens. Self-consistent approach to deformation of intruder states in neutron-deficient Pb and Po. *Phys. Lett. B*, 569:151–158, 2003.
- [13] A. Frank, P. Van Isacker, and C.E. Vargas. Evolving shape coexistence in the lead isotopes: the geometry of configuration mixing in nuclei. *Phys. Rev. C*, 69:034323, 2004.
- [14] V. Hellemans, S. De Bardemacker, and K.H. Heyde. Configuration mixing in the neutron-deficient  $^{186-196}\text{Pb}$  isotopes. *Phys. Rev. C*, 77:064324, 2008.
- [15] T. Grahn, A. Dewald, O. Möller, R. Julin, C.W. Beausang, S. Christen, I.G. Darby, S. Eeckhaudt, P.T. Greenlees, A. Görgen, K. Helriutta, J. Jolie, P. Jones, S. Juutinen, H. Kettunen, T. Kröll, R. Krücken, Y. Le Coz, M. Leino, A.-P. Leppänen, P. Maierbeck, D.A. Meyer, B. Melon, P. Nieminen, M. Nyman, R.D. Page, J. Pakarinen, P. Petkov, P. Rahkila, B. Saha, M. Sanzeliuss, J. Sarén, C. Scholey, J. Uusitalo, M. Bender, and P.-H. Heenen. Lifetimes of intruder states in  $^{186}\text{Pb}$ ,  $^{188}\text{Pb}$  and  $^{194}\text{Po}$ . *Nucl. Phys. A*, 801:83–100, 2008.
- [16] H. De Witte, A.N. Andreyev, N. Barré, M. Bender, T.E. Cocolios, S. Dean, D. Fedorov, V.N. Fedoseyev, L.M. Fraile, S. Franchoo, V. Hellemans, P.-H. Heenen, K. Heyde, G. Huber, M. Huyse, H. Jeppessen, U. Köster, P. Kunz, S.R. Leshner, B. A. Marsh, I. Mukha, B. Roussière, J. Sauvage, M. Seliverstov, I. Stefanescu, E. Tengborn, K. Van de Vel, J. Van de Walle, P. Van Duppen, and Yu. Volkov. Nuclear charge radii of neutron deficient lead isotopes beyond  $N=104$  mid-shell investigated by in-source laser spectroscopy. *Phys. Rev. Lett.*, 98:112502, 2007.
- [17] M.D. Seliverstov, A.N. Andreyev, N. Barré, A.E. Barzakh, S. Dean, H. De Witte, D.V. Fedorov, V.N. Fedoseyev, L.M. Fraile, S. Franchoo, J. Genevey, G. Huber, M. Huyse, U. Köster, P. Kunz, S.R. Leshner, B.A. Marsh, I. Mukha, B. Roussière, J. Sauvage, I. Stefanescu, K. Van de Vel, P. Van Duppen, and Yu.M. Volkov. Charge radii and magnetic moments of odd- $A$   $^{183-189}\text{Pb}$  isotopes. *Eur. Phys. J. A*, 41:315–321, 2009.
- [18] P. Van Duppen, E. Coenen, K. Deneffe, Huyse M., K. Heyde, and P. Van Isacker. Observation of low-lying  $J^\pi = 0^+$  states in the single-closed-shell nuclei  $^{192-198}\text{Pb}$ . *Phys. Rev. Lett.*, 52:1974–1977, 1984.
- [19] E. Coenen, K. Deneffe, M. Huyse, P. Van Duppen, and J.L. Wood.  $\alpha$  decay of neutron-deficient odd Bi nuclei: shell-model intruder states in Tl and Bi isotopes. *Phys. Rev. Lett.*, 54:1783–1786, 1985.
- [20] P. Van Duppen, E. Coenen, K. Deneffe, and M. Huyse.  $\beta^+$ /electron-capture decay of  $^{192,194,196,198,200}\text{Bi}$ : experimental evidence for low lying  $0^+$  states. *Phys. Rev. C*, 35:1861–1877, 1987.
- [21] J.C. Griffin, R.A. Braga, R.W. Fink, J.L. Wood, H.K. Carter, R.L. Mlekodaj, C.R. Bingham, E. Coenen, M. Huyse, and P. Van Duppen. Decay of mass-separated 3.0 min  $^{195g}\text{Bi}$  to levels in  $^{195}\text{Pb}$  and shape coexistence in the neutron-deficient odd-mass Pb isotopes. *Nucl. Phys. A*, 530:401–419, 1991.
- [22] J. Vanhorenbeeck, P. Del Marmol, E. Coenen, M. Huyse, P. Van Duppen, and J. Wauters. Highly converted transitions in  $^{197}\text{Pb}$ : evidence for shape coexistence. *Nucl. Phys. A*, 531:63–76, 1991.
- [23] T.E. Cocolios, B.A. Marsh, V.N. Fedosseev, S. Franchoo, G. Huber, M. Huyse, A.M. Ionan,

- K. Johnston, U. Köster, Yu. Kudryavtsev, M.D. Seliverstov, E. Noah, T. Stora, and P. Van Duppen. Resonant laser ionization of polonium at rilis-isolde for the study of ground-en isomer-state properties. *Nucl. Intr. and Meth. B*, 266:4403–4406, 2008.
- [24] R.M. Diamond and F.S. Stephens. Isomeric levels in the light thallium isotopes. *Nucl. Phys.*, 45:632–646, 1963.
- [25] J.F. Ziegler. SRIM-2003. *Nucl. Intr. and Meth. B*, 219-220:1027–1036, 2004.
- [26] Zh. Chunmei. Nuclear data sheets for  $A = 195$ . *Nucl. Data Sheets*, 86:645–784, 1999.
- [27] A.M. Andreyev, K. Van de Vel, A. Barzakh, A. De Smet, H. De Witte, V.N. Fedorov, V.N. Fedoseyev, S. Franchoo, M. Gòrska, M. Huyse, Z. Janas, U. Köster, W. Kurcewicz, J. Kurpeta, V.I. Mishin, K. Partes, A. Plochocki, P. Van Duppen, and L. Weissman. Nuclear spins, magnetic moments and  $\alpha$ -decay spectroscopy of long-lived isomeric states in  $^{185}\text{Pb}$ . *Eur. Phys. J. A*, 14:63–75, 2002.
- [28] J. Wauters, P. Dendoovern, M. Huyse, G. Reusen, P. Van Duppen, and P. Lievens. Alpha decay properties of neutron-deficient polonium and radon nuclei. *Phys. Rev. C*, 47:1447–1454, 1993.
- [29] J. Wauters, P. Decrock, P. Dendooven, M. Huyse, P. Lievens, G. Reusen, and P. Van Duppen. The influence of recoil losses in subsequent  $\alpha$  decay on the determination of  $\alpha$ -branching ratios. *Nucl. Intr. and Meth. B*, 61:178–182, 1991.
- [30] P. Hornshøj, B. Jonson, H.L. Ravn, L. Westgaard, and O.B. Nielsen. Widths for  $s$ - and  $d$ -wave  $\alpha$ -decay of neutron-deficient isotopes with  $Z \leq 82$ . *Nucl. Phys. A*, 230:365–379, 1974.
- [31] J.O. Rasmussen. Alpha-decay barrier penetrabilities with an exponential nuclear potential: even-even nuclei. *Phys. Rev.*, 113:1593–1598, 1959.
- [32] J. Wauters, P. Dendooven, P. Decrock, M. Huyse, R. Kirchner, O. Klepper, G. Reusen, E. Roeckl, and P. Van Duppen. The alpha-branching ratios of the  $^{188,190,192}\text{Pb}$  isotopes. *Z. Phys. A*, 342:277–282, 1992.
- [33] J. Bonn, G. Huber, H.-J. Kluge, U. Köpf, L. Kugler, and E.-W. Otten. Optical pumping of neutron deficient  $^{187}\text{Hg}$ . *Nucl. Phys. A*, 230:365–379, 1974.
- [34] S.B. Dutta, R. Kirchner, O. Klepper, T.U. Köhl, D. Marx, G.D. Sprouse, R. Menges, U. Dinger, G. Huber, and S. Schröder. Measurement of the isotope shift and hyperfine splitting of  $^{190,191,193,197}\text{Pb}$  isotopes by collinear laser spectroscopy. *Z. Phys. A*, 341:39–45, 1991.
- [35] R. Arvieu, O. Bohigas, and C. Quesne. Analysis of the properties of the odd-mass single closed shell nuclei with a surface delta interaction. *Nucl. Phys. A*, 143:577–601, 1970.